DOCHERTY, N.J., and CHANSON, H. (2012). "Physical Modelling of Unsteady Turbulence in Breaking Tidal Bores." *Journal of Hydraulic Engineering*, ASCE, Vol. 138, No. 5, pp. 412-419 (DOI: 10.1061/(ASCE)HY.1943-7900.0000542) (ISSN 0733-9429).

PHYSICAL MODELLING OF UNSTEADY TURBULENCE IN BREAKING TIDAL BORES

Nicholas J. Docherty ([1]) and Hubert Chanson ([2]) ([*])

([1]) The University of Queensland, School of Civil Engineering, Brisbane QLD 4072, Australia

([2]) The University of Queensland, School of Civil Engineering, Brisbane QLD 4072, Australia

([*]) Corresponding author, Ph.: (61 7) 3365 4163, Fax: (61 7) 3365 4599, E-mail: h.chanson@uq.edu.au

Abstract: A tidal bore is an unsteady flow motion generated by the rapid water level rise at the river mouth during the early flood tide under macro-tidal and appropriate bathymetric conditions. The present study investigates physically the turbulent properties of tidal bores. The results are based upon some experimental measurements of free-surface fluctuations and turbulent velocities conducted on smooth and rough beds. The free-surface measurements were conducted with Froude numbers between 1 and 1.7. Both undular and breaking bores were observed. Using an ensemble-averaging technique, the free-surface fluctuations of breaking tidal bores are characterised. Immediately prior to the roller, the free-surface curves gradually upwards. The passage of the bore roller is associated with some large water elevation fluctuations; the largest free-surface fluctuations are observed during the first half of the bore roller. The turbulent velocity measurements were performed at several vertical elevations during and shortly after the passage of breaking bores. Both the instantaneous and ensemble-averaged velocity data highlight a strong flow deceleration at all elevations during the bore passage. Close to the bed, the longitudinal velocity component becomes negative immediately after the roller passage implying the existence of a transient recirculation. The height and duration of the transient is a function of the bed roughness, with a longer and higher recirculation region above the rough bed. The vertical velocity data presented some positive, upward motion beneath the front with increasing maximum vertical velocity with increasing distance from the bed. The transverse velocity data show some large fluctuations with non-zero ensemble-average after the roller passage that highlight some intense secondary motion advected behind the bore front.

Keywords: Breaking tidal bores, Turbulence, Physical modelling, Free-surface fluctuations, Ensemble-averaged velocity components.

INTRODUCTION

A tidal bore is an unsteady flow motion generated by the rapid water level rise at the river mouth during the early flood tide. With time, the leading edge of the tidal wave becomes steeper until it forms a wall of water: i.e., the tidal bore. After the formation of the bore, there is a discontinuity in water depth and velocity field at the bore front (Fig. 1). Once formed, the flow properties immediately in front and behind the tidal bore must satisfy the continuity and momentum principles (Rayleigh 1908, Henderson 1966, Liggett 1994, Chanson 2012). The integral form of the equations of conservation of mass and momentum gives some relationship

between the flow properties in front of and behind the bore front. For an observer travelling at the surge speed U in a rectangular horizontal channel and neglecting bed friction, the quasi-steady flow analogy yields:

$$\frac{d_{conj}}{d_o} = \frac{1}{2}\left(\sqrt{1+8Fr^2} - 1\right) \quad (1)$$

where d_o is the initial water depth, d_{conj} is the downstream conjugate flow depth immediately after the bore passage, V_o is the initial river flow velocity positive downstream, and U is the tidal bore celerity for an observer standing on the bank positive upstream (Fig. 2). Fr is the tidal bore Froude number defined as:

$$Fr = \frac{V_o + U}{\sqrt{g\,d_o}} \quad (2)$$

The tidal bore Froude number Fr is always greater than unity. For Fr < 1, the tidal wave cannot transform into a tidal bore. The tidal bore front is a turbulent unsteady flow motion that is comparable to a shock (Lighthill 1978). Figure 1 shows a small tidal bore.

Despite some recent advances (Hornung et al. 1995, Koch and Chanson 2009, Chanson 2010), the knowledge into the unsteady turbulent motion in a tidal bore remains limited. The present study investigates physically the turbulent flow properties of tidal bores. The analysis is based upon some experimental measurements of free-surface fluctuations and turbulent velocities conducted in a relatively large facility on smooth and rough beds. It is the aim of this work to characterise the unsteady turbulent velocity fields in breaking tidal bores.

PHYSICAL MODELLING OF TIDAL BORES

PRESENTATION

The laboratory studies of tidal bores are performed with geometrically similar models for which the geometric scaling ratio L_r is defined as the ratio of prototype to model dimensions. The physical modelling requires the selection of an adequate similitude. For a tidal bore propagating in a horizontal, rectangular channel, a simplified dimensional analysis yields:

$$d, V_x, V_y, V_z = F_1(x, y, z, t, U, d_o, V_o, \delta, B, g, \rho, \mu, \sigma...) \quad (3)$$

where d is the flow depth, V_x, V_y, V_z are respectively the longitudinal, transverse and vertical velocity components at a location (x, y, z), x is the coordinate in the flow direction, y is the horizontal transverse coordinate measured from the channel centreline, z is the vertical coordinate measured from channel bed, t is the time, U is the surge celerity, V_o is the initial flow velocity, δ is the boundary layer thickness at x, B is the channel width, g is the gravity acceleration, ρ and μ are the water density and dynamic viscosity respectively, and σ is the surface tension between air and water. Equation (3) expresses the flow properties (left handside terms) at a position (x, y, z) and at a time t as functions of the tidal bore properties, initial flow properties, channel geometry and fluid properties. In addition, the biochemical properties of the water solution may be considered especially in natural estuarine systems.

For a tidal bore, the theoretical considerations showed that the relevant characteristic length and velocity scales are respectively the initial flow depth d_o and (V_o+U) (Eq. (1) & (2)). Equation (3) may be rewritten in dimensionless terms:

$$\frac{d}{d_o}, \frac{V_x}{V_o}, \frac{V_y}{V_o}, \frac{V_z}{V_o} = F_2\left(\frac{x}{d_o}, \frac{y}{d_o}, \frac{z}{d_o}, t\sqrt{\frac{g}{d_o}}, \frac{V_o + U}{\sqrt{g d_o}}, \rho \times \frac{(V_o + U) d_o}{\mu}, \frac{\delta}{d_o}, \frac{B}{d_o}, \frac{g \mu^4}{\rho \sigma^3}, ...\right) \quad (4)$$

In Equation (4) right handside, the fifth and sixth terms are the tidal bore Froude and Reynolds numbers respectively, and the ninth term is the Morton number which is a function only of fluid properties and gravity constant.

In a geometrically similar model, a true dynamic similarity is achieved only if each dimensionless parameter has the same value in both model and prototype. Scale effects may exist when one or more Π-terms have different values between the model and prototype. In free-surface flows including tidal bores, the gravity effects are important and a Froude similitude is commonly used (Henderson 1966, Chanson 1999). That is, the model and prototype Froude numbers must be equal. But the turbulent mixing processes are dominated by viscous forces implying the needs for a Reynolds similitude. Figure 1 illustrates indeed the turbulence of a tidal bore front. For geometrically-similar tidal bore models, it is impossible to satisfy simultaneously all the similarities because of too many relevant parameters (Eq. (4)). In practice, the physical studies are based upon a Froude similitude, but no systematic study was conducted to date to ascertain any scale effect affecting the turbulent mixing in tidal bore flows. It is worth noting that the above analysis (Eq. (4)) does not account for the physio-chemical properties of the water, the air entrainment in the bore roller nor the characteristics of any intrusive instrumentation. The present study focused on some basic laboratory experiments performed under controlled flow conditions in a relatively large size flume based upon a Froude similitude. The experimental configuration was selected to minimise potential viscous scaling effects by selecting large initial depths and velocities, and Reynolds numbers (Table 1).

EXPERIMENTAL FACILITY AND INSTRUMENTATION

The experiments were performed in a 12 m long, 0.5 m wide tilting flume (Fig. 3). The channel was made of smooth PVC bed and glass walls. The water was supplied by a constant head tank to a large intake chamber with a smooth convergent feeding into the glass-walled channel. A fast-closing gate was located at the channel downstream end. Two experimental configurations were tested. One series of experiments was conducted on the smooth PVC invert. For the other series of experiments, the bed was covered with plywood sheets covered by natural blue granite gravels which were sieved between 4.75 mm and 6.70 mm, glued in resin and covered by a spray gloss surface finish. The hydraulic roughness of the gravel bed was tested in steady gradually-varied flows and the equivalent Darcy friction factor was f = 0.036 on average, corresponding to an equivalent sand roughness height k_s = 3.4 mm. Table 1 summarises the range of experimental flow conditions for the free-surface measurements where Q is the initially steady flow rate, and S_o is the bed slope. Note that, for 1.4 < Fr < 1.6, the flow conditions corresponded to a 5:1 scale study of the

bore seen in Figure 1.

The flow rate was measured with two orifice meters that were calibrated on site with a volume per time technique. In steady flows, the water depths were measured using rail mounted pointer gauges. The unsteady water depths were recorded using several acoustic displacement meters Microsonic™ Mic+25/IU/TC with an accuracy of 0.2 mm. The turbulent velocity measurements were performed with an acoustic Doppler velocimeter (ADV) Nortek™ Vectrino+ equipped with a three-dimensional side-looking head (Fig. 3B). The velocity range was set to 1.0 m/s, and the data accuracy was 1% of velocity range (i.e. 0.01 m/s). The translation of the ADV probe in the vertical direction was controlled by a fine adjustment travelling mechanism connected to a Mitutoyo™ digimatic scale unit with an error less than 0.1 mm. Herein all the measurements were taken on the channel centreline, and the ADV and displacement sensors were synchronised within 1 ms and sampled simultaneously at 200 Hz.

During some preliminary experiments, recurrent problems were observed with the velocity data, including low correlations and low signal to noise ratios, because of the inadequate seeding of the channel water. Thereafter, and for all the study, the channel water was seeded with 100 g of clay powder per hour of operation. The clay powder was introduced in the intake structure and was dispersed progressively with time. Further the unsteady flow post-processing was limited to a removal of communication errors following Koch and Chanson (2009) and Chanson (2010), and it is acknowledged that the vertical velocity component Vz data might be affected adversely by the bed proximity for $z < 0.030$ m. This is further discussed and documented in Docherty and Chanson (2010), together with more detailed information on the experimental apparatus.

INFLOW CONDITIONS AND TIDAL BORE GENERATION

For each experimental run, the initially steady flow conditions were established for 5 minutes prior to the first measurements. The tidal bore was generated by the rapid partial closure of the downstream gate. The gate closure time was less than 0.15 s. After closure, the bore propagated upstream (Fig. 3) and each experiment was stopped before the bore front reached the channel upstream end to avoid any wave reflection effect. The ADV measurements were conducted at $x = 5$ m downstream of the channel upstream end. In steady flows, some detailed velocity measurements indicated that the flow was partially-developed at $x = 5$ m: $\delta/d_o = 0.47$ and 0.64 for smooth bed and fixed gravel bed respectively.

For each series of experiments, the free-surface properties were documented (Table 1). Then some detailed velocity measurements were conducted in breaking bores at $x = 5$ m for $0.005 < z/d_o < 0.77$. On the gravel bed, z was measured above the top of the gravel materials using a semi-circular footing with a 25.1 cm^2 area. At a number of vertical elevations, a series of twenty instantaneous velocity records were repeated with the same well-defined initially-steady flow conditions. An ensemble-median of each instantaneous velocity component was calculated.

FREE-SURFACE MEASUREMENTS

The free-surface observations highlighted two types of tidal bores depending upon the Froude number Fr. For a Froude number between unity and 1.5, the tidal bore was undular: that is, the tidal bore front was followed by a train of secondary, quasi-periodic waves called undulations. For larger Froude numbers (Fr > 1.5 to 1.6), a breaking bore with a marked roller was observed (Fig. 3). The findings were identical for smooth and rough bed, and they were comparable to those of earlier studies (Treske 1994, Hornung et al. 1995, Koch and Chanson 2009).

For tidal bore Froude numbers less than 1.5, the bore consisted of first wave followed by a train of well-formed undulations. The wave amplitude a_w and steepness a_w/L_w data are summarised in Table 1 (columns 10 & 11), together with the conjugate depth d_{conj} (column 8) and maximum water depth d_{max} at the first wave crest (column 9). The dimensionless wave steepness data are presented in Figure 4. In Figure 4, the data were compared with laboratory observations, as well as with the linear wave theory solution of Lemoine (1948) and the Boussinesq equation solution of Andersen (1978). For a bore Froude number slightly larger than unity, the wave steepness increased monotically with an increasing Froude number Fr to a local maximum followed by a sharp decrease immediately before the disappearance of free-surface undulations. The observations were consistent with earlier data as seen in Figure 4.

For a tidal bore with a marked roller (Fr = 1.5-1.6), the visual observations showed that the flow was basically two-dimensional and the free-surface properties were systematically investigated by repeating 25 identical experiments and the results were ensemble-averaged (Fig. 5). The flow conditions could be considered as a 5:1 scale study ($L_r = 5$) of the tidal bore seen in Figure 1. Both the free-surface and the visual observations showed that the free-surface elevation rose first slowly, immediately prior to the roller (Fig. 5 & 6). This is sketched in Figure 6 where the period Δt_1 corresponded to the duration of the gentle rise h_s of the free-surface with $h_s/d_o \approx 0.1$ (Table 2). Such a gradual rise in free-surface ahead of the turbulent roller was previously observed by Hornung et al. (1995) and Koch and Chanson (2009). Immediately after, the turbulent roller caused by a sharp rise in water depth that was basically a discontinuity (Fig. 5). This corresponded to the period Δt_2 sketched in Figure 6. The characteristic free-surface length and time scale data are summarised in Table 2.

Figure 5 present the time-variations of the ensemble-averaged median water depth and fluctuations for both smooth and gravel beds. Each graph includes the ensemble-averaged median water depth d_{median}, and the differences between 3rd and 4th quartiles (d_{75}-d_{25}) and 90% and 10% percentiles (d_{90}-d_{10}). Both (d_{75}-d_{25}) and (d_{90}-d_{10}) characterised the free-surface fluctuations around the median value. The data showed that the free-surface fluctuations were the largest next to the roller toe and impingement point, and they decayed quasi-exponentially with increasing time as the bore roller passed beneath the sensor. Typically the maximum free-surface fluctuations were observed during the first half of the bore roller with $\Delta t_3/\Delta t_2 \approx 0.48$ (Fig. 5), and the observation was consistent with the findings of Mouaze et al. (2005) and Murzyn and Chanson (2009) in stationary hydraulic jumps.

UNSTEADY VELOCITY MEASUREMENTS

In a tidal bore with a marked roller, the turbulent velocity measurements showed that the arrival of the tidal bore and the sudden increase in water depth yielded a rapid change in the longitudinal velocity component to satisfy the conservation of mass. The longitudinal velocities were characterised by a rapid flow deceleration at all vertical elevations, while some large fluctuations of longitudinal, transverse and vertical velocity components were observed beneath the tidal bore. The tidal bore was a hydrodynamic shock characterised by a sudden change in the velocity field (Lighthill 1978). The front was followed by a highly turbulent flow motion with significant fluctuations of all velocity components. Some typical Eulerian measurements are presented in Figure 7. Figure 7 shows the instantaneous free-surface elevation, longitudinal and vertical velocity components as function of time.

An ensemble-median of each instantaneous velocity component was produced at selected vertical elevations. Some typical results are presented also in Figure 7 and compared with the instantaneous data for a experiment (Run 1). Both the instantaneous and ensemble-averaged (EA) data showed some key features of the unsteady turbulence in breaking tidal bores. These included a rapid flow deceleration during the passage of the tidal bore roller above the sampling volume, some negative longitudinal velocity component next to the bed (Fig. 7A & 7B) highlighting some transient recirculation "bubble", and some positive vertical velocity component beneath the roller (Fig. 7C & 7D). The latter was believed to be closely linked with the streamline curvature immediately prior to the bore roller.

The experimental results showed that the passage of the roller was associated with some large free-surface fluctuations (Fig. 5), and linked with some large longitudinal velocity fluctuations and some transient upwards flow motion ($V_z > 0$) (Fig. 8). Figure 8 presents the differences between the 3rd and 4th quartiles (V_{75}-V_{25}) and 90% and 10% percentiles (V_{90}-V_{10}), for the longitudinal and transverse velocity components, that gave a measure of the turbulent velocity fluctuations. The maximum horizontal velocity fluctuations occurred about the same time as when the maximum free-surface fluctuations were observed. Further the transverse velocity data V_y presented some large fluctuations after the bore front for $z/d_o \geq 0.43$, typically 5 to 10 times $\sqrt{g/d_o}$ after the front passage (Fig. 8B). The findings implied some intense secondary motion in the wake of the tidal bore front.

Interestingly, the vertical velocity data V_z presented a substantial positive value during the front passage for $z/d_o \geq 0.43$ (Fig. 7C & 7D). It is believed to be closely linked with the streamline curvature immediately prior to the bore roller ($t < t_s$) and possibly during the roller propagation. Since the free-surface is a streamline, the surface slope is related to the vertical velocity component at the free-surface:

$$\frac{V_z(z=d)}{V_x(z=d)} = \frac{\partial d}{\partial x} \quad (5)$$

where $V_x(z=d)$ is the horizontal velocity component at the surface while, at the bed, $V_z(z=0) = 0$ for an impervious boundary. For a solitary wave, Boussinesq (1871) assumed a linear distribution of vertical

velocity:

$$\frac{V_z}{V_z(z=d)} = \frac{z}{d} \quad (6)$$

The result may be applied to open channel flows with streamline curvature (Montes 1998). In the present study, the magnitude of the maximum median vertical velocity component $(V_z)_{max}$ increased with increasing distance from the bed (Fig. 7C & 7D). This is illustrated in Figure 9 showing the maximum median vertical velocity component as a function of the vertical elevation. On the same graph, the free-surface elevation rate $(\partial d/\partial t)_{z=d}$ is shown in addition. Since $V_z(z=0) = 0$ at the bed and $V_z(z=d) = (\partial d/\partial t)_{z=d}$ at the free-surface, an entire data trend can be extrapolated and the present data were best correlated by:

$$\left(\frac{V_z}{V_o}\right)_{max} = 0.215 \times \frac{z}{d_o} \quad \text{for } 0 < z/d < 1 \text{ on smooth PVC} \quad (7)$$

$$\left(\frac{V_z}{V_o}\right)_{max} = 0.466 \times \left(\frac{z}{d_o}\right)^{1.54} \quad \text{for } 0 < z/d < 1 \text{ on fixed gravel} \quad (8)$$

with a normalised correlation coefficient of 0.982 and 0.999 for Equations (7) and (8) respectively (Fig. 9). The smooth bed data (Eq. (7)) corresponded to Boussinesq's (1871) approximation (Eq. (6)), while the gravel bed data yielded a similar monotonic relationship but with a different power law exponent (Eq. (8)) & Fig. 9).

DISCUSSION

The experimental results highlighted simply a quantitative difference between the smooth and rough beds, not only in the initially steady flow but also during the unsteady bore motion as seen in Figure 6. These might be linked with slightly different flow conditions (Table 1), but may also be associated with some effects of the bed roughness on the turbulent flow field, especially close to the bed.

The results showed that the passage of a breaking bore is characterised by large turbulent velocity fluctuations at all vertical elevations including next to the bed (Fig. 6). When the breaking tidal bore propagates upstream in a river, the natural river bed is subjected to a rapid flow reversal during the transient recirculation, associated with large fluctuations of all velocity components (Fig. 7 & 8) beneath and behind the bore roller. Next to the bed, the large velocity gradients associated with the velocity fluctuations induce some large turbulent shear stresses, while the bed is subjected to significant velocity reversals associated with some cyclic loading. The natural bed material consists typically cohesive sediments which are saturated, and the changes in pore pressures may induce some liquefaction, contributing to the upwards advection of bed material into the water column. The advected material is then transported upstream by the breaking bore (Fig. 2B). Figure 2B shows a sketch of the natural bed scour behind a breaking tidal bore.

The present findings highlighted the drastic impact of a tidal bore onto the estuarine process. In turn, any man-made intervention leading to the disappearance of the tidal bore may have adverse impacts onto the natural eco-system. For example, the bores of the Seine and Couesnon Rivers in France no longer exist after

respectively extensive training works and dredging, and the construction of upstream barrage (Chanson 2011).

CONCLUSION

The unsteady turbulence in tidal bores was investigated physically under controlled conditions with two types of bed roughness: smooth PVC and fixed gravel bed. Some free-surface measurements were conducted with tidal bore Froude numbers between 1 and 1.7. Both undular and breaking bores were observed. The tidal bore flow patterns were independent of the bed roughness. The free-surface properties were close to earlier findings. Using an ensemble-averaging technique, the free-surface fluctuations of breaking tidal bores were characterised. Immediately prior to the roller, the free-surface curved gradually upwards and the gentle surface elevation rise was about $0.1d_o$ where d_o is the initial water depth. The passage of the bore roller was associated with some large water depth fluctuations; the largest free-surface fluctuations were observed during the first half of the bore roller.

Some detailed turbulent velocity measurements were performed at several vertical elevations during and shortly after the passage of breaking bores. Both the instantaneous and ensemble-averaged velocity data highlighted some seminal features. That is, a strong flow deceleration was observed at all elevations during the tidal bore passage. Close to the bed, the longitudinal velocity component became negative immediately after the roller passage implying the existence of a transient recirculation. The height and duration of the transient was a function of the bed roughness, with a longer and higher recirculation region above the rough bed. The vertical velocity data presented some positive, upward motion during the bore passage with increasing maximum vertical velocity with increasing distance from the bed. The vertical motion was believed to be linked with some streamline curvature in front of the roller. The transverse velocity data presented some large fluctuations with non-zero ensemble-average after the roller passage that highlighted some intense secondary motion advected behind the bore.

ACKNOWLEDGEMENTS

The authors thank Graham Illidge and Clive Booth (The University of Queensland) for their technical assistance. They thank further Prof. Colin Apelt (The University of Queensland), Prof. Laurent David (University of Poitiers, France) and Dr David Reungoat (University of Bordeaux, France) for their valuable comments.

REFERENCES

Andersen, V.M. (1978). "Undular Hydraulic Jump." *Jl of Hyd. Div.*, ASCE, Vol. 104, No. HY8, pp. 1185-1188. Discussion : Vol. 105, No. HY9, pp. 1208-1211.

Boussinesq, J.V. (1871). "Théorie de l'Intumescence appelée Onde Solitaire ou de Translation se Propageant dans un Canal Rectangulaire." ('Theory of the Solitary Wave propagating in an Rectangular Channel.') *Comptes-Rendus de l'Académie des Sciences*, Paris, France, Vol. 72, pp. 755-759.

DOCHERTY, N.J., and CHANSON, H. (2012). "Physical Modelling of Unsteady Turbulence in Breaking Tidal Bores." *Journal of Hydraulic Engineering*, ASCE, Vol. 138, No. 5, pp. 412-419 (DOI: 10.1061/(ASCE)HY.1943-7900.0000542) (ISSN 0733-9429).

Chanson, H. (1999). "The Hydraulics of Open Channel Flow: An Introduction." *Edward Arnold*, London, UK, 512 pages.

Chanson, H. (2010). "Unsteady Turbulence in Tidal Bores: Effects of Bed Roughness." *Journal of Waterway, Port, Coastal, and Ocean Engineering*, ASCE, Vol. 136, No. 5, pp. 247-256 (DOI: 10.1061/(ASCE)WW.1943-5460.0000048).

Chanson, H. (2011). "Tidal Bores, Aegir, Eagre, Mascaret, Pororoca: Theory and Observations." *World Scientific*, Singapore, 220 pages.

Chanson, H. (2012). "Momentum Considerations in Hydraulic Jumps and Bores." *Journal of Irrigation and Drainage Engineering*, ASCE, Vol. 138 (DOI 10.1061/(ASCE)IR.1943-4774.0000409) (in Print).

Docherty, N.J., and Chanson, H. (2010). "Characterisation of Unsteady Turbulence in Breaking Tidal Bores including the Effects of Bed Roughness." *Hydraulic Model Report No. CH76/10*, School of Civil Engineering, The University of Queensland, Brisbane, Australia, 112 pages (ISBN 9781864999884).

Henderson, F.M. (1966). "Open Channel Flow." *MacMillan Company*, New York, USA.

Hornung, H.G., Willert, C., and Turner, S. (1995). "The Flow Field Downstream of a Hydraulic Jump." *Jl of Fluid Mech.*, Vol. 287, pp. 299-316.

Koch, C., and Chanson, H. (2009). "Turbulence Measurements in Positive Surges and Bores." *Journal of Hydraulic Research*, IAHR, Vol. 47, No. 1, pp. 29-40 (DOI: 10.3826/jhr.2009.2954).

Lemoine, R. (1948). "Sur les Ondes Positives de Translation dans les Canaux et sur le Ressaut Ondulé de Faible Amplitude." ('On the Positive Surges in Channels and on the Undular Jumps of Low Wave Height.') *Jl La Houille Blanche*, Mar-Apr., pp. 183-185 (in French).

Liggett, J.A. (1994). "Fluid Mechanics." *McGraw-Hill*, New York, USA.

Lighthill, J. (1978). "Waves in Fluids." *Cambridge University Press*, Cambridge, UK, 504 pages.

Montes, J.S. (1998). "Hydraulics of Open Channel Flow." *ASCE Press*, New-York, USA, 697 pages.

Mouaze, D., Murzyn, F., and Chaplin, J.R. (2005). "Free Surface Length Scale Estimation in Hydraulic Jumps." *Jl of Fluids Eng.*, Trans. ASME, Vol. 127, pp. 1191-1193.

Murzyn, F., and Chanson, H. (2009). "Free-Surface Fluctuations in Hydraulic Jumps: Experimental Observations." *Experimental Thermal and Fluid Science*, Vol. 33, No. 7, pp. 1055-1064 (DOI: 10.1016/j.expthermflusci.2009.06.003).

Rayleigh, Lord (1908). "Note on Tidal Bores." *Proc. Royal Soc. of London, Series A containing Papers of a Mathematical and Physical Character*, Vol. 81, No. 541, pp. 448-449.

Treske, A. (1994). "Undular Bores (Favre-Waves) in Open Channels - Experimental Studies." *Jl of Hyd. Res.*, IAHR, Vol. 32, No. 3, pp. 355-370. Discussion: Vol. 33, No. 3, pp. 274-278.

NOTATION

a_w wave amplitude (m);

B channel width (m);

d (a) flow depth (m) measured normal to the invert;

(b) flow depth (m) measured above the fixed gravel bed;

d_{conj} conjugate flow depth (m) measured immediately behind the tidal bore front;

d_{max} flow depth (m) at the first wave crest;

d_o initial flow depth (m) measured normal to the chute invert;

Fr tidal bore Froude number defined as: $Fr = (V_o + U) / \sqrt{g \times d_o}$;

f Darcy-Weisbach friction factor;

g gravity constant (m/s^2): g = 9.80 m/s^2 in Brisbane, Australia;

h_s rise in free-surface elevation (m) in front of the breaking bore front (Fig. 6);

k_s equivalent sand roughness height (m);

L_r geometric scaling ratio;

L_w wave length (m) measured from crest to crest;

Q volume flow rate (m^3/s);

Re tidal bore Reynolds number: $Re = \rho(V_o+U)d_o/\mu$;

S_o bed slope: $S_o = \sin\theta$;

t time (s);

U tidal bore front celerity (m/s) for an observer standing on the bank, positive upstream;

V_o initial flow velocity (m/s) positive downstream: $V_o = q/d_o$;

V_x longitudinal velocity (m/s) positive downstream;

V_y transverse velocity (m/s) positive towards the left sidewall;

V_z vertical velocity (m/s) positive upwards;

x longitudinal distance (m) measured from the channel upstream end, positive downstream;

y transverse distance (m) measured from the channel centreline, positive towards the left sidewall;

z distance (m) normal to the bed; it is the vertical distance (m) for a horizontal channel; for the fixed ravel bed, z is measured above the top of the gravel bed;

Greek symbols

Δt_1, Δt_2, Δt_3 characteristic periods (s) of the breaking bore front (Fig. 6);

δ boundary layer thickness (m) defined in terms of 99% of the free-stream velocity;

μ dynamic viscosity (Pa.s);

θ bed slope angle with the horizontal, positive downwards;

ρ water density (kg/m^3);

σ surface tension between air and water (Pa.s);

Subscript

conj conjugate flow conditions: i.e., immediately behind the tidal bore front;

median median value (i.e. 50% percentile);

x	longitudinal component positive downstream;
y	component transverse to the channel centreline;
z	component normal to the invert;
o	initial flow conditions : i.e., upstream of the positive surge front;
10	10% percentile;
25	25% percentile;
75	75% percentile;
90	90% percentile;

Abbreviations

ADV	acoustic Doppler velocimeter;

Notation

$\partial/\partial z$	partial differentiation with respect to z.

DOCHERTY, N.J., and CHANSON, H. (2012). "Physical Modelling of Unsteady Turbulence in Breaking Tidal Bores." *Journal of Hydraulic Engineering*, ASCE, Vol. 138, No. 5, pp. 412-419 (DOI: 10.1061/(ASCE)HY.1943-7900.0000542) (ISSN 0733-9429).

Table 1 - Free-surface properties of tidal bores (Present study)

Bed roughness	Q (m^3/s)	S_o	d_o (**) (m)	Fr	Re	Type of tidal bore	d_{conj}/d_o	d_{max}/d_o	a_w/d_o	a_w/L_w
(1)	(2)	(3)	(4)	(5)	(6)	(7)	(8)	(9)	(10)	(11)
Smooth PVC bed	0.050	0	0.119	1.65	$1.9\ 10^5$	Breaking	1.88	N/A	N/A	N/A
			0.117	1.59	$1.8\ 10^5$	Breaking	1.93	N/A	N/A	N/A
			0.117	1.44	$1.8\ 10^5$	Undular/breaking	1.58	1.72	0.141	0.018
			0.117	1.36	$1.7\ 10^5$	Undular	1.45	1.71	0.234	0.032
			0.116	1.24	$1.5\ 10^5$	Undular	1.36	1.61	0.186	0.027
			0.117	1.11	$1.4\ 10^5$	Undular	1.22	1.33	0.096	0.013
			0.117	1.08	$1.3\ 10^5$	Undular	1.10	1.18	0.074	0.005
Fixed gravel bed	0.050	0.002	0.125 (*)	1.52	$1.6\ 10^5$	Undular/breaking	1.71	1.93	0.193	0.028
			0.125 (*)	1.45	$1.6\ 10^5$	Undular	1.48	1.75	0.280	0.040
			0.125 (*)	1.40	$1.5\ 10^5$	Undular	1.48	1.77	0.285	0.046
			0.125 (*)	1.24	$1.4\ 10^5$	Undular	1.32	1.45	0.149	0.019
			0.125 (*)	1.17	$1.3\ 10^5$	Undular	1.23	1.29	0.069	0.008
			0.125 (*)	1.01	$1.1\ 10^5$	Undular	1.13	1.13	0.023	0.001

Notes: a_w: wave amplitude of first wave length; d_o: initial water depth; d_{conj}: conjugate depth; d_{max}: water depth of first wave crest; Fr: tidal bore Froude number; L_w first wave length; Q: discharge; Re: Bore Reynolds number; S_o: bed slope; (*): measured above the roughness; (**) measured at x = 5 m; All data were recorded at x = 5 m.

Table 2 - Breaking bore free-surface elevation time and length scale (breaking tidal bore on horizontal channel)

Reference	Q	d_o (**)	Fr	Bed roughness	h_s/d_o	$\sqrt{\frac{g}{d_o}}\Delta t_1$	$\sqrt{\frac{g}{d_o}}\Delta t_2$	$\sqrt{\frac{g}{d_o}}\Delta t_3$
	(m^3/s)	(m)						
(1)	(2)	(3)	(4)	(5)	(6)	(7)	(8)	(9)
Koch & Chanson (2009)	0.040	0.079	1.75-1.9	Smooth PVC	0.10	--	--	--
Chanson (2010)	0.058	0.137	1.50	Smooth PVC	0.116	2.71	2.03	--
		0.142 (*)	1.46	Plastic screens (k_s = 6.6 mm)	0.107	3.41	2.16	--
Present study (***)	0.050	0.119	1.65	Smooth PVC	0.080	3.18	4.36	1.63
		0.127 (*)	1.50	Fixed gravel bed (k_s = 3.4 mm)	0.150	2.81	3.16	1.93

Notes: (*): measured above the roughness; (**) measured at x = 5 m; (***): ensemble-averaged data; (--): data not available.

DOCHERTY, N.J., and CHANSON, H. (2012). "Physical Modelling of Unsteady Turbulence in Breaking Tidal Bores." *Journal of Hydraulic Engineering*, ASCE, Vol. 138, No. 5, pp. 412-419 (DOI: 10.1061/(ASCE)HY.1943-7900.0000542) (ISSN 0733-9429).

LIST OF CAPTIONS

Fig. 1 - Photographs of the tidal bore of the Sélune River (France) on 1 September 2008 (Fr ~ 1.4-1.6, Re ~ 2×10^6) - Bore propagation from left to right - Photograph by Hubert Chanson

Fig. 2 - Definition sketch of tidal bores
(A) Undular bore propagating upstream
(B) River bed scour beneath a breaking tidal bore

Fig. 3 - Breaking tidal bores in the laboratory channel
(A) Looking downstream at the advancing breaking bore roller: Q = 0.050 m^3/s, d_o = 0.120 m, Fr = 1.58, Re = 2.0×10^5, fixed gravel bed, shutter: 1/60 s
(B) Bore propagation from left to right: Q = 0.050 m^3/s, d_o = 0.125 m, Fr = 1.5, Re = 1.9×10^5, fixed gravel bed, shutter: 1/100 s - Note the underwater bubble "trail" behind the bore roller (Left) and the ADV head on the right

Fig. 4 - Dimensionless wave steepness a_w/L_w as a function of the undular tidal bore Froude number - Comparison between the present undular bore data, earlier laboratory studies (Treske 1994, Koch and Chanson 2009, Chanson 2010), the linear wave theory (Lemoine 1948) and Boussinesq equation (Andersen 1978)

Fig. 5 - Ensemble-average median water depth d_{median}, difference between 3rd and 4th quartiles (d_{75}-d_{25}) and 90% and 10% percentiles (d_{90}-d_{10}) in a breaking tidal bore
(A) Fr = 1.65, Re = 2.1×10^5, Q = 0.0499 m^3/s, d_o = 0.119 m, Smooth PVC bed data
(B) Fr = 1.50, Re = 1.7×10^5, Q = 0.0500 m^3/s, d_o = 0.127 m, Fixed gravel bed data

Fig. 6 - Sketch of median and fluctuations of water depth in a breaking bore front

Fig. 7 - Free-surface and turbulent velocity measurements under a breaking tidal bore - Flow conditions: (A & C) smooth PVC bed, Fr = 1.6, Re = 2.0×10^5, d_o = 0.118 m, Q = 0.050 m^3/s; (B & D) fixed gravel bed, Fr = 1.5, Re = 2.1×10^5, d_o = 0.126 m, Q = 0.050 m^3/s
(A, Left) z/d_o = 0.135, smooth PVC bed
(B, Right) z/d_o = 0.135, fixed gravel bed
(C, Left) z/d_o = 0.733, smooth PVC bed
(D, Left) z/d_o = 0.733, fixed gravel bed

Fig. 8 - Ensemble-average median velocity component V_{median}, difference between 3rd and 4th quartiles (V_{75}-

V_{25}) and 90% and 10% percentiles (V_{90}-V_{10}), and ensemble-average median water depth d_{median} - Q = 0.050 m^3/s, d_o = 0.117 m, Fr = 1.6, Re = 2.0×10^6, z/d_o = 0.434, smooth PVC bed

(A) Longitudinal velocity component V_x

(B) Transverse velocity component V_y

Fig. 9 - Maximum median vertical velocity beneath the tidal bore roller and corresponding free-surface vertical velocity on smooth PVC and fixed gravel beds - Flow conditions: (a) smooth PVC bed, Fr = 1.6, Re = 2.0×10^5, d_o = 0.118 m, Q = 0.050 m^3/s; (b) fixed gravel bed, Fr = 1.5, Re = 2.1×10^5, d_o = 0.126 m, Q = 0.050 m^3/s - Comparison with Equations (7) and (8)

DOCHERTY, N.J., and CHANSON, H. (2012). "Physical Modelling of Unsteady Turbulence in Breaking Tidal Bores." *Journal of Hydraulic Engineering*, ASCE, Vol. 138, No. 5, pp. 412-419 (DOI: 10.1061/(ASCE)HY.1943-7900.0000542) (ISSN 0733-9429).

Fig. 1 - Photographs of the tidal bore of the Sélune River (France) on 1 September 2008 (Fr ~ 1.4-1.6, Re ~ 2×10^6) - Bore propagation from left to right - Photograph by Hubert Chanson

DOCHERTY, N.J., and CHANSON, H. (2012). "Physical Modelling of Unsteady Turbulence in Breaking Tidal Bores." *Journal of Hydraulic Engineering*, ASCE, Vol. 138, No. 5, pp. 412-419 (DOI: 10.1061/(ASCE)HY.1943-7900.0000542) (ISSN 0733-9429).

Fig. 2 - Definition sketch of tidal bores

(A) Undular bore propagating upstream

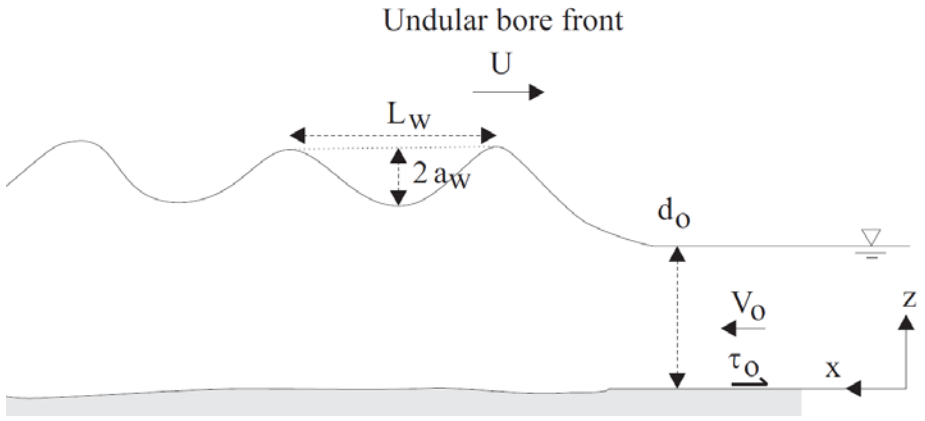

(B) River bed scour beneath a breaking tidal bore

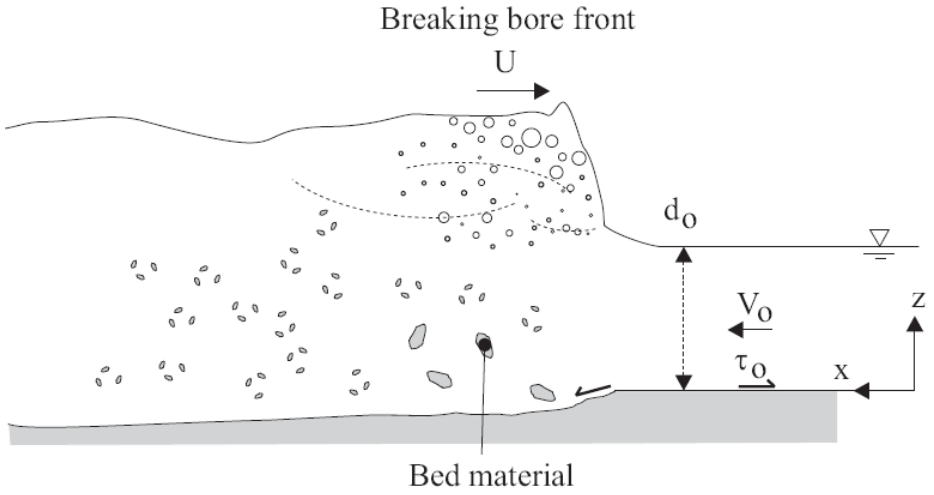

DOCHERTY, N.J., and CHANSON, H. (2012). "Physical Modelling of Unsteady Turbulence in Breaking Tidal Bores." *Journal of Hydraulic Engineering*, ASCE, Vol. 138, No. 5, pp. 412-419 (DOI: 10.1061/(ASCE)HY.1943-7900.0000542) (ISSN 0733-9429).

Fig. 3 - Breaking tidal bores in the laboratory channel

(A) Looking downstream at the advancing breaking bore roller: Q = 0.050 m^3/s, d_o = 0.120 m, Fr = 1.58, Re = 2.0×10^5, fixed gravel bed, shutter: 1/60 s

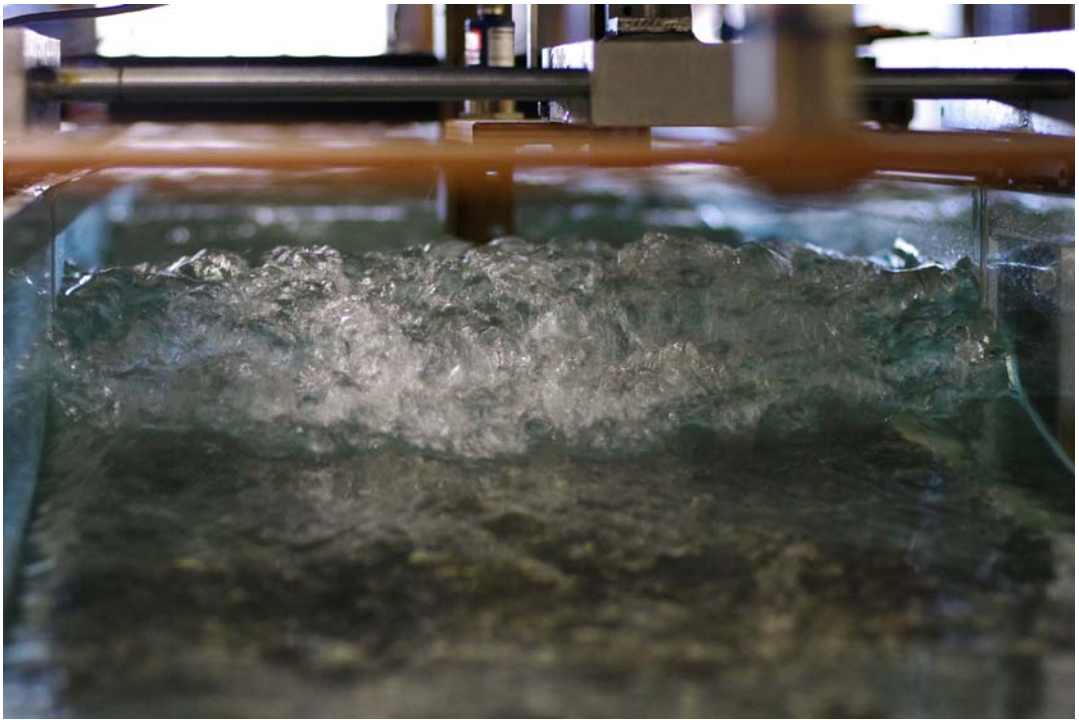

(B) Bore propagation from left to right: Q = 0.050 m^3/s, d_o = 0.125 m, Fr = 1.5, Re = 1.9×10^5, fixed gravel bed, shutter: 1/100 s - Note the underwater bubble "trail" behind the bore roller (Left) and the ADV head on the right

DOCHERTY, N.J., and CHANSON, H. (2012). "Physical Modelling of Unsteady Turbulence in Breaking Tidal Bores." *Journal of Hydraulic Engineering*, ASCE, Vol. 138, No. 5, pp. 412-419 (DOI: 10.1061/(ASCE)HY.1943-7900.0000542) (ISSN 0733-9429).

Fig. 4 - Dimensionless wave steepness a_w/L_w as a function of the undular tidal bore Froude number - Comparison between the present undular bore data, earlier laboratory studies (Treske 1994, Koch and Chanson 2009, Chanson 2010), the linear wave theory (Lemoine 1948) and Boussinesq equation (Andersen 1978)

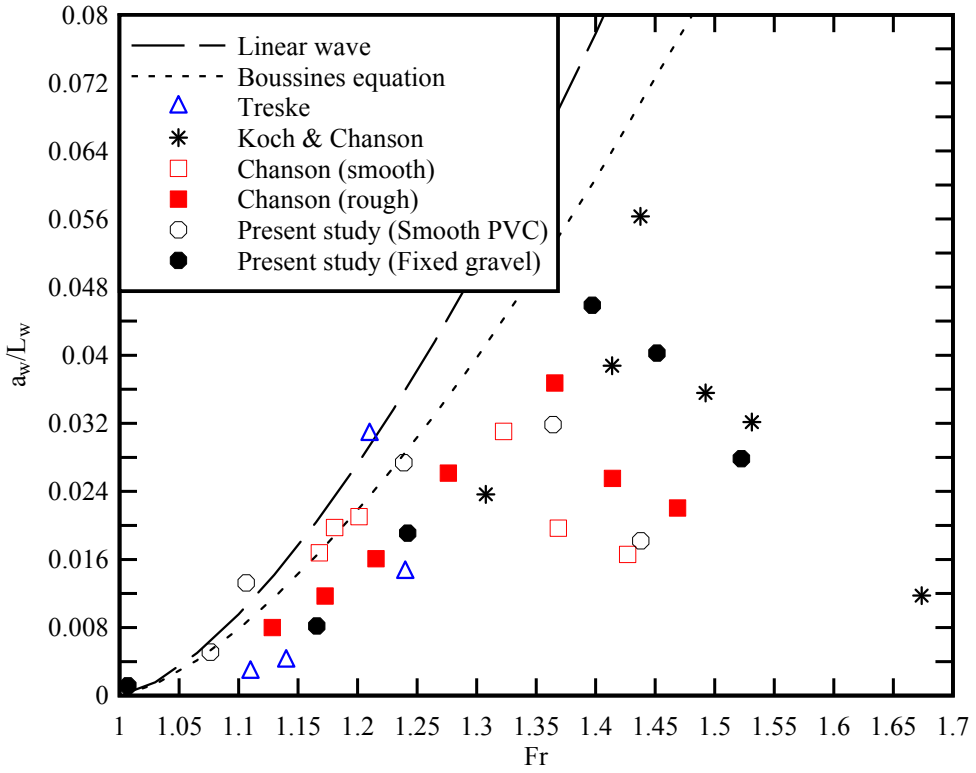

DOCHERTY, N.J., and CHANSON, H. (2012). "Physical Modelling of Unsteady Turbulence in Breaking Tidal Bores." *Journal of Hydraulic Engineering*, ASCE, Vol. 138, No. 5, pp. 412-419 (DOI: 10.1061/(ASCE)HY.1943-7900.0000542) (ISSN 0733-9429).

Fig. 5 - Ensemble-average median water depth d_{median}, difference between 3rd and 4th quartiles (d_{75}-d_{25}) and 90% and 10% percentiles (d_{90}-d_{10}) in a breaking tidal bore

(A) Fr = 1.65, Re = 2.1×10^5, Q = 0.0499 m^3/s, d_o = 0.119 m, Smooth PVC bed data

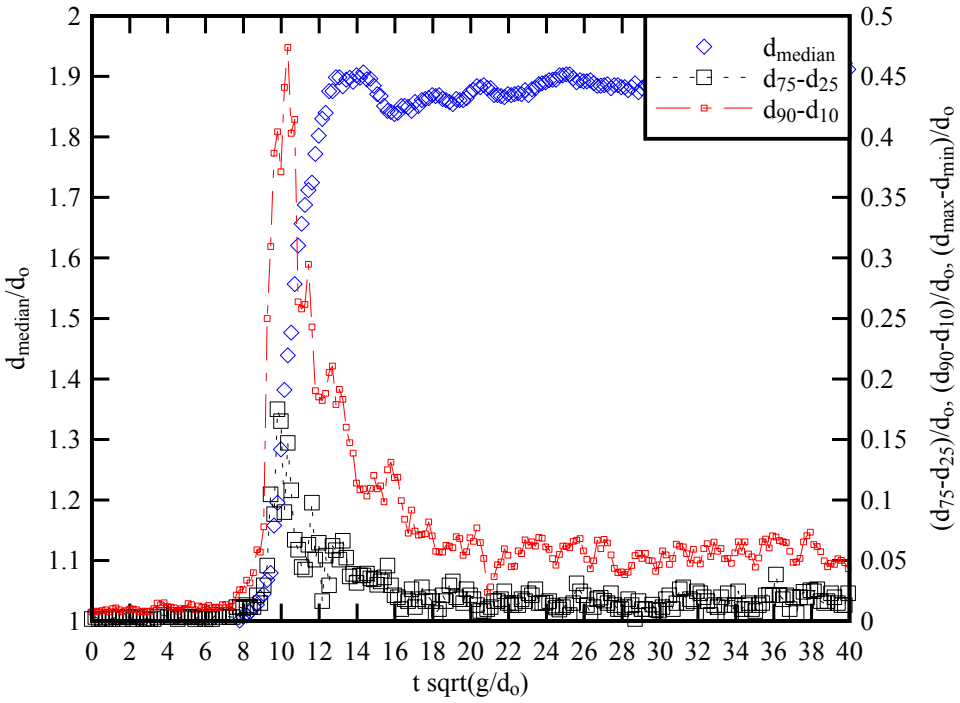

(B) Fr = 1.50, Re = 1.7×10^5, Q = 0.0500 m^3/s, d_o = 0.127 m, Fixed gravel bed data

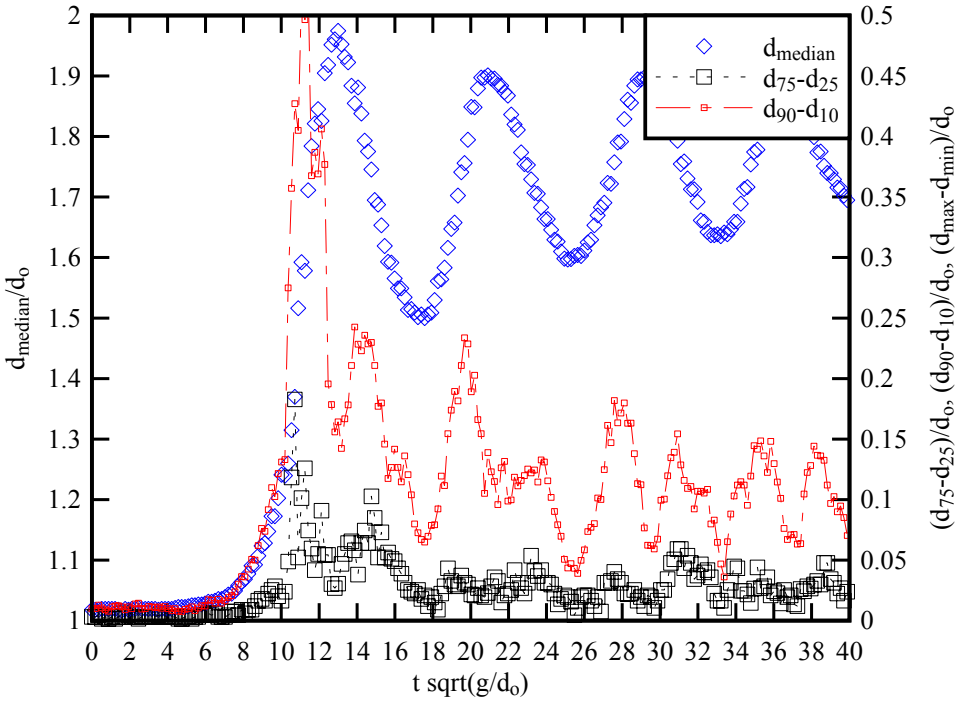

DOCHERTY, N.J., and CHANSON, H. (2012). "Physical Modelling of Unsteady Turbulence in Breaking Tidal Bores." *Journal of Hydraulic Engineering*, ASCE, Vol. 138, No. 5, pp. 412-419 (DOI: 10.1061/(ASCE)HY.1943-7900.0000542) (ISSN 0733-9429).

Fig. 6 - Sketch of median and fluctuations of water depth in a breaking bore front

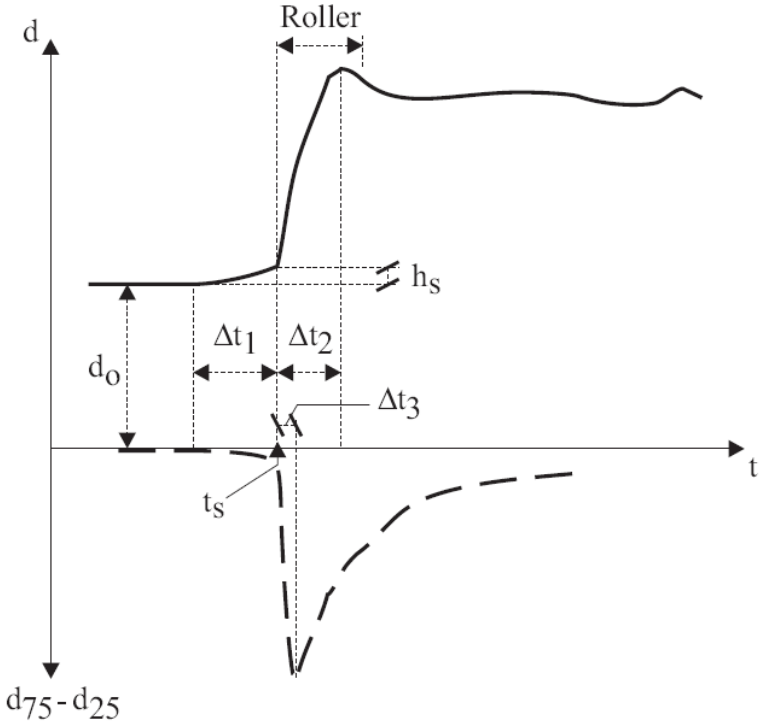

DOCHERTY, N.J., and CHANSON, H. (2012). "Physical Modelling of Unsteady Turbulence in Breaking Tidal Bores." *Journal of Hydraulic Engineering*, ASCE, Vol. 138, No. 5, pp. 412-419 (DOI: 10.1061/(ASCE)HY.1943-7900.0000542) (ISSN 0733-9429).

Fig. 7 - Free-surface and turbulent velocity measurements under a breaking tidal bore - Flow conditions: (A & C) smooth PVC bed, Fr = 1.6, Re = 2.0×10^5, d_o = 0.118 m, Q = 0.050 m^3/s; (B & D) fixed gravel bed, Fr = 1.5, Re = 2.1×10^5, d_o = 0.126 m, Q = 0.050 m^3/s

(A, Left) z/d_o = 0.135, smooth PVC bed

(B, Right) z/d_o = 0.135, fixed gravel bed

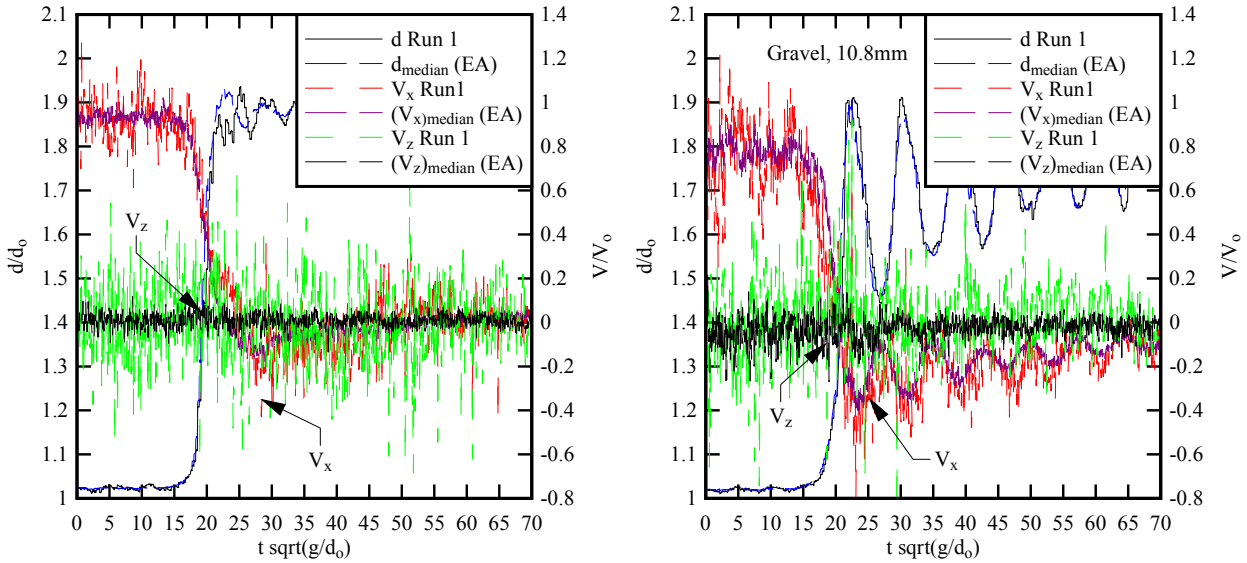

(C, Left) z/d_o = 0.733, smooth PVC bed

(D, Left) z/d_o = 0.733, fixed gravel bed

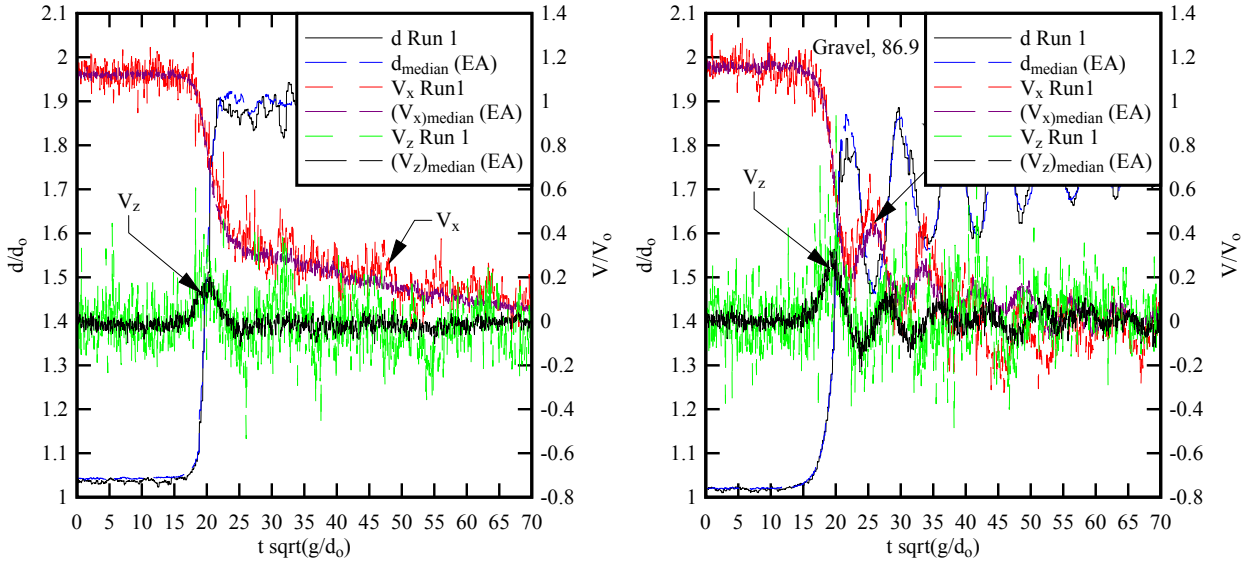

DOCHERTY, N.J., and CHANSON, H. (2012). "Physical Modelling of Unsteady Turbulence in Breaking Tidal Bores." *Journal of Hydraulic Engineering*, ASCE, Vol. 138, No. 5, pp. 412-419 (DOI: 10.1061/(ASCE)HY.1943-7900.0000542) (ISSN 0733-9429).

Fig. 8 - Ensemble-average median velocity component V_{median}, difference between 3rd and 4th quartiles (V_{75}-V_{25}) and 90% and 10% percentiles (V_{90}-V_{10}), and ensemble-average median water depth d_{median} - Q = 0.050 m^3/s, d_o = 0.117 m, Fr = 1.6, Re = 2.0×10^6, z/d_o = 0.434, smooth PVC bed

(A) Longitudinal velocity component V_x

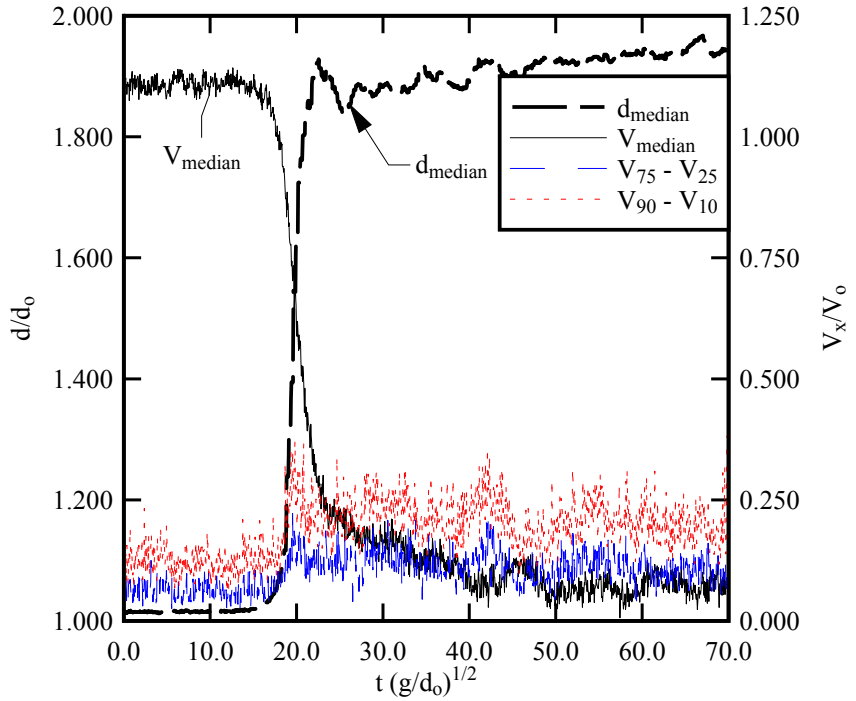

(B) Transverse velocity component V_y

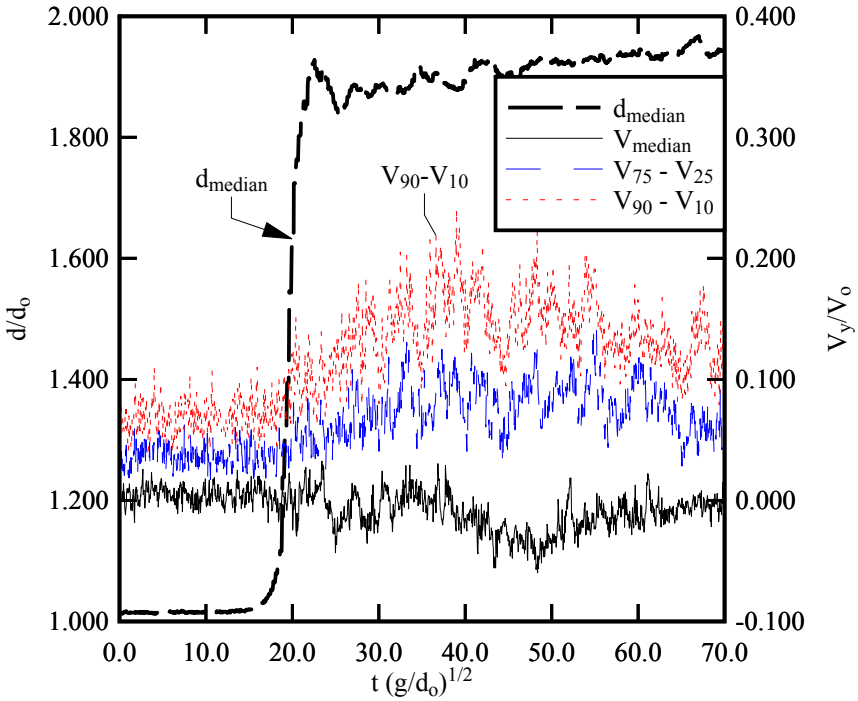

DOCHERTY, N.J., and CHANSON, H. (2012). "Physical Modelling of Unsteady Turbulence in Breaking Tidal Bores." *Journal of Hydraulic Engineering*, ASCE, Vol. 138, No. 5, pp. 412-419 (DOI: 10.1061/(ASCE)HY.1943-7900.0000542) (ISSN 0733-9429).

Fig. 9 - Maximum median vertical velocity beneath the tidal bore roller and corresponding free-surface vertical velocity on smooth PVC and fixed gravel beds - Flow conditions: (a) smooth PVC bed, Fr = 1.6, Re = 2.0×10^5, d_o = 0.118 m, Q = 0.050 m^3/s; (b) fixed gravel bed, Fr = 1.5, Re = 2.1×10^5, d_o = 0.126 m, Q = 0.050 m^3/s - Comparison with Equations (7) and (8)